



**HAL**  
open science

## Performance of portable TDCR systems developed at LNE-LNHB

Benoît Sabot, Chavdar Dutsov, Philippe Cassette, Krasimir Mitev

► **To cite this version:**

Benoît Sabot, Chavdar Dutsov, Philippe Cassette, Krasimir Mitev. Performance of portable TDCR systems developed at LNE-LNHB. Nuclear Instruments and Methods in Physics Research Section A: Accelerators, Spectrometers, Detectors and Associated Equipment, 2021, 1034, pp.166721. 10.1016/j.nima.2022.166721 . cea-03713381

**HAL Id: cea-03713381**

**<https://cea.hal.science/cea-03713381v1>**

Submitted on 4 Jul 2022

**HAL** is a multi-disciplinary open access archive for the deposit and dissemination of scientific research documents, whether they are published or not. The documents may come from teaching and research institutions in France or abroad, or from public or private research centers.

L'archive ouverte pluridisciplinaire **HAL**, est destinée au dépôt et à la diffusion de documents scientifiques de niveau recherche, publiés ou non, émanant des établissements d'enseignement et de recherche français ou étrangers, des laboratoires publics ou privés.



Distributed under a Creative Commons Attribution - NonCommercial 4.0 International License



## Performance of portable TDCR systems developed at LNE-LNHB

Benoît Sabot<sup>a,\*</sup>, Chavdar Dutsov<sup>b</sup>, Philippe Cassette<sup>b</sup>, Krasimir Mitev<sup>b</sup>

<sup>a</sup> Université Paris-Saclay, CEA, LIST, Laboratoire National Henri Becquerel (LNE-LNHB), F-91120 Palaiseau, France

<sup>b</sup> Sofia University "St. Kliment Ohridski", Faculty of Physics, 5 James Bourchier Blvd, 1164, Bulgaria

### ARTICLE INFO

#### Keywords:

Liquid scintillation  
Scintillation counter  
TDCR  
Radionuclide metrology

### ABSTRACT

The triple to double coincidence ratio (TDCR) liquid scintillation measurement technique is commonly used in national metrology institutes (NMIs) to perform standardization of pure beta emitters. The LNE-LNHB historical device, RCTD1, is a quite large device, which has been developed and commonly used over the past 30 years with its associated electronics for measurements of various radionuclides. During the last 4 years LNE-LNHB has developed two new portable TDCR devices. Such portable instrumentation gives end-users access to a reference measurement method that can be used for a large number of radionuclides. It addresses a wide range of industrial and medical applications for radionuclide metrology, including calibrations of solutions containing short-lived radionuclides, avoidance of radioactive source transportation, and performing on-site comparison to promote radionuclide metrology harmonization. In this paper, we will present the newly developed portable TDCR liquid scintillation measurement systems. Two kinds of devices have been developed and designed at LNE-LNHB and built using fused deposition modelling (FDM) 3D printing: a mini-TDCR (25 cm diameter, 10 cm height) and a micro-TDCR (16 cm diameter, 10 cm height). After a detailed discussion of the design and the possibilities offered by 3D printing for their conception, this paper will present the performance of the devices obtained for several radionuclides. The results will be compared with the RCTD1 in order to validate the performance of the new devices. They exhibit improved performance, such as higher detection efficiency, and include various useful tools for proper on-site metrology. The first tests, which were performed in Orsay Hospital (CEA/SHFJ) and in another laboratory (IRSN), allowed us to show the very good overall performance of the systems including their outstanding linearity, which was tested in the range from  $430\,000\text{ s}^{-1}$  down to  $160\text{ s}^{-1}$  in the double coincidences channel. Applications of the developed systems for high and low activity measurements are also discussed. Finally, the portable device has been used for half-life measurements in order to check for impurities in a radio-pharmaceutical solution.

### 1. Introduction

The triple-to-double coincidence ratio (TDCR) technique is a direct measurement method regarded by the international metrology community as a primary measurement technique for many radionuclides (pure beta or alpha emitter, electron capture, etc.) [1]. The measurand is the activity of the scintillating source, which can be traced to the mass activity of the solution if the scintillating sources are prepared by precision weighing. The radionuclides that can be calibrated by this method are those for which it is possible to estimate the energy spectrum absorbed by the scintillating source following a decay. In general, for the simplest decay schemes (i.e. a pure beta emitter that decays directly to the ground state) the TDCR measurement is easier than for a complex scheme, and for highest detection efficiency the TDCR measurement is more accurate as it is less dependent on the model. This concerns in particular radionuclides decaying by a pure beta transition or by electron capture to the fundamental level of the

daughter nucleus. Application of the TDCR method requires the use of three photomultiplier tubes (PMTs). The design of such a device with high detection efficiency is a key prerequisite for high accuracy measurements, and achieving this was one of the primary goals of this work.

Previous studies performed by different national metrology institutes (NMIs), including the Laboratoire National Henri Becquerel (LNE-LNHB) from the Commissariat à l'Énergie Atomique (CEA), have shown the importance of having portable TDCR devices in order to perform on-site calibrations, especially for the measurement of  $^3\text{H}$  in nuclear power plants [2]. In addition, some radionuclides, such as those used for positron emission tomography examinations ( $^{18}\text{F}$  with a half-life of 1.8 h;  $^{11}\text{C}$  with a half-life of 20 min;  $^{15}\text{O}$  with a half-life of 2 min), are difficult to transfer from the production site (typically a Hospital equipped with a cyclotron) to an NMI for primary calibration because of their short half-life. Hence the requirement for on-site primary

\* Corresponding author.

E-mail address: [benoit.sabot@cea.fr](mailto:benoit.sabot@cea.fr) (B. Sabot).



Fig. 1. 3D illustration of the mini-TDCR device. Its large size is due to additional components that can be included in the system: an external photon-emitting source with a collimator and a gamma detector (NaI(Tl) or Ce(Br) 0.5 inch size and CdTe). With these components the system can be used as a Compton spectrometer.

measurement techniques in order to comply with French regulation [3]. A primary measurement technique available on site will not only allow calibration of the dose calibrator in the numerous geometries required in the radiopharmaceutical production laboratory, but also, provide an on-site technique to respond to specific metrology requests for the development of new radiopharmaceuticals, such as alpha emitters or those decaying by electron capture.

Secondly, for some radionuclides such as  $^{222}\text{Rn}$  in water, where the half-life is longer (3.8232 d), source transportation, preparation and sampling are quite complex, requiring on-site calibration of the liquid scintillation counters. In practice, transportation and regulations related to the use of radioactive sources are becoming more and more difficult [4], so having on-site capability, involving the use of a transportable and reference device, becomes a useful tool for metrology purposes.

Finally, with the recent development of the Extended International Reference System for pure  $\beta$ -particle emitting radionuclides (ESIR) [5], we believe that such a well-known and well characterized portable device could be used for portable reference systems similar to the International Reference System Transfer Instrument (SIR-TI) [6]. ESIR and SIR-TI aim to demonstrate the international equivalence of primary standards from NMIs, so that such portable TDCR devices could be used in the same way as travelling instruments between NMIs.

This work presents the progress made in the last four years, starting in 2016, for the conception and validation of two portable TDCR devices. After a detailed description of the devices and their properties, their validation will be discussed with different comparisons performed in the laboratory with the historical device RCTD1 [7] and associated electronics [8]. In addition, on-site comparisons with a portable device [9] of a laboratory from Sofia University “St. Kliment Ohridski”, Bulgaria (SUBG), will be presented. Finally, on-site measurements with the developed devices are presented and discussed.

## 2. Materials and methods

The two measurement devices have been designed and developed at LNE-LNHB. The first one, named mini-TDCR, is based on the feedback of a previous study which had shown that the Hamamatsu R7600U photo-multiplier tubes (PMTs) proposed by the Italian Metrology Institute (ENEA) [2] seemed to be well suited to the design of such devices. A specific feature of the mini-TDCR is the inclusion of a Compton-TDCR system [10] with gamma spectrometer. The second one, named micro-TDCR, uses new and more efficient Hamamatsu H11234-203 MOD PMTs and is a more compact device.

### 2.1. Design considerations

The design of the two portable instruments was primarily oriented by the geometry of the selected PMTs in order to maximize the detection efficiency. To do so, the following characteristics and assumptions were considered:

- Typical measurement sample: 20 mL liquid scintillation vial. Among all types of vials available in the laboratory (glass, plastic, etc.), the maximum external diameter is less than 28 mm, and the maximum height with the cap is 68 mm. The position of the meniscus in a vial filled to 10 mL is 20 mm above the bottom of the vial.
- The meniscus of the liquid scintillation vial, with a 10 mL filling, was placed in the centre of the PMTs to maximize light collection. The light output at the meniscus level is strong as the light is totally reflected at the liquid-air interface.
- In order to minimize light loss between the emission point and the PMTs, the distance between the sample and the PMT window was optimized to account for their small size.
- The addition of different neutral density filters may be necessary to vary the detection efficiency; therefore, sufficient space was provided to accommodate these filters between the vial and the PMTs.
- The shape of the optical chamber is optimized to favour reflection of the light and direct it towards the PMTs.
- The system is compact and includes a miniature high voltage power supply, equipped with a safety device to avoid damaging the PMTs during a sample change. This safety device turns off the high voltage if the apparatus is opened, allowing light to enter.
- The instrument must allow for easy sample changing, while being perfectly light-tight once the measurement has started.
- The device must not be sensitive to surrounding electromagnetic fields and is therefore shielded against these disturbances.
- The thresholds of the photomultipliers must be easily adjustable in order to allow the detection of single photons, a condition inherent to the measurement method.
- It must be possible to easily combine the TDCR devices with other detectors in order to perform coincidence measurements or to use a Compton spectrometer.

The limitations being well established, new ways of production were considered in view of the complexity of the elements required, not necessarily achievable by standard manufacturing. The laboratory has thus been equipped with FDM 3D printers [11]. The FDM technique, which consists of adding material deposited by fusion, offers the best quality/versatility/price ratio possible with 3D printing. More than a hundred readily available materials can be used with this technique. The printed parts do not require any treatment, and the use of

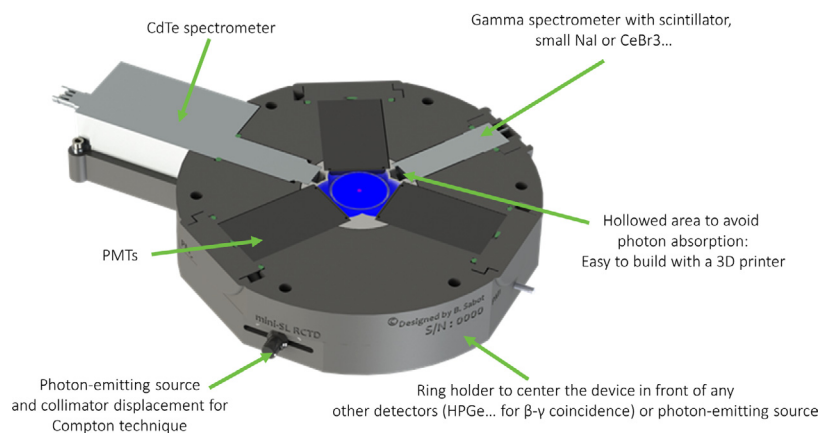


Fig. 2. 3D picture of the mini-TDCR: this cut, normal to the z axis shows the position of the vial and the other detectors.

commercial 3D printers is relatively trouble-free. This manufacturing process allows complex shapes to be produced which are not easy to manufacture using computer numerical controlled (CNC) machining. At the very least, with machining, it would be necessary to break down the main parts of the system into several parts to be manufactured and assembled. Hence, the design of the optical chamber and enclosure was developed assuming that everything could be produced by 3D printing.

Prior to the design of the detector, studies were performed on the different materials available for 3D printing, resulting in polylactic acid (PLA) filaments been chosen, mainly because of their availability in both white and black, which facilitates the printing of opaque material.

The drawback with this printing technique is the fabrication method, which consists of fusing filaments in successive layers whose thicknesses range from  $25\ \mu\text{m}$  to  $300\ \mu\text{m}$ . Each layer is made of  $400\ \mu\text{m}$  wide molten plastic fibres fused together side by side. It appears that thin PLA layers are partially transparent to light. This effect is due either to the material thickness or to light passing between two fibres that may not be fused properly. In our case, we have observed that it was necessary to have a minimum thickness of 2 mm of PLA to avoid external light penetration.

## 2.2. Mini-TDCR system

The mini-TDCR (Fig. 1) uses three Hamamatsu R7600U-200 PMTs [12] with an ultra bi-alkali photocathode. The supply voltage is positive so that the photocathode is at ground potential, which reduces the background noise [13]. The PMTs provide good quantum efficiency with a maximum of 40% for wavelengths between 300 nm and 650 nm, which is compatible with the emission spectrum of liquid scintillators.

The face of the PMTs is 30 mm square, and they are 53 mm long. These dimensions allow them to be brought as close as possible to the light source, i.e. the 20 mL scintillation vial, as shown by the cross-section in Fig. 2. A diffusive layer of adhesive tape is placed on the PMT windows to minimize optical reflections due to the difference between the refractive indices of air and glass. The active surface of these PMTs is an 18 mm square, so a large part of the PMT window is insensitive to light.

As can be seen in Fig. 2, 3D printing allows the formation of recesses, which are used here to minimize the absorption of radiation in the materials of the measuring device, especially for the gamma detectors integrated in this mini-TDCR device.

## 2.3. Micro-TDCR system

The micro-TDCR uses Hamamatsu H11934-203 PMTs [14] with a 30 mm square window and a depth of 32 mm. The sensitive surface is a 23 mm square, larger than the previous PMTs. These PMTs also have an ultra bi-alkali photocathode like the preceding ones, with the same



Fig. 3. Exploded view of micro-TDCR, the components of the device are all inside producing a very compact device.

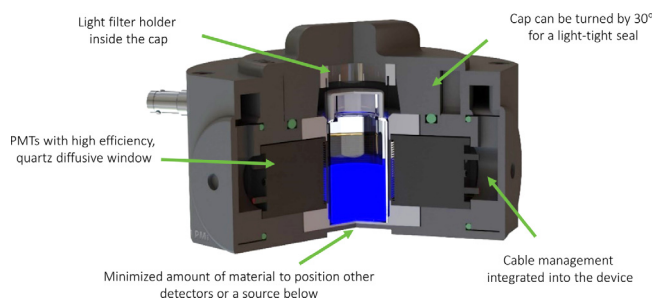


Fig. 4. 3D picture of the micro-TDCR device, the most efficient and compact system.

quantum efficiency, but the window of the PMTs is made of quartz and is diffusive. The smaller size of these PMTs allows a smaller device to be built, as shown in Fig. 4.

Compared to the mini-TDCR, the micro-TDCR cannot accommodate any other detectors and is only intended for standard TDCR measurements. A 3D vertical cross section of this micro-TDCR with the vial position are shown in Fig. 3. The meniscus of the vial is placed in the middle of the PMT in order to collect maximum light. The minimum distance between the vial wall and the PMT is 1 mm, allowing sufficient space to place neutral density filters as described below. Below the vial, the material height is 2 mm in order to prevent light from entering the chamber. As can be seen in Fig. 5, only six different 3D printed parts are needed to build the device and the components are inside the enclosure. The optical chamber is made of a different material and can easily be exchanged.

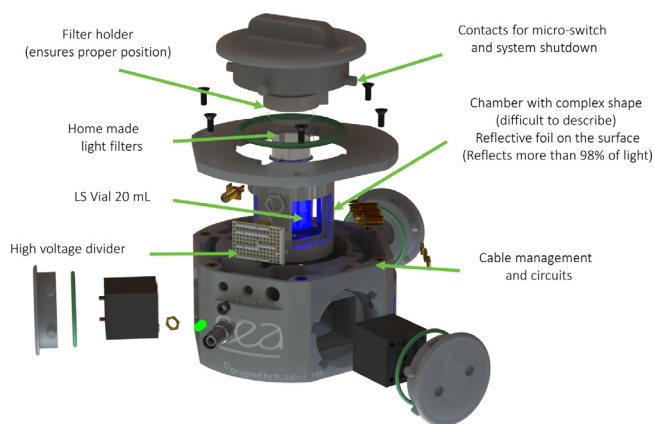


Fig. 5. Exploded view of micro-TDCR, the components of the device are all inside producing a very compact device.

#### 2.4. Optical chamber

Both devices, mini-TDCR and micro-TDCR, use photomultipliers with the same window sizes and accommodate the same types of liquid scintillation vials (20 mL). Consequently their optical chambers have been designed with exactly the same shape and dimensions and the vial-PMT distance are identical for both version of the TDCR.

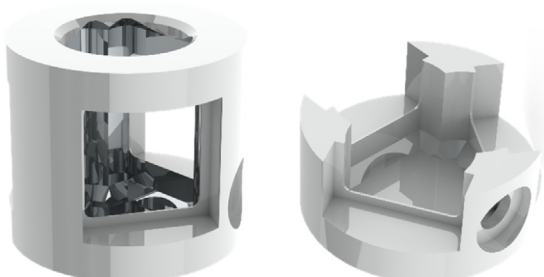


Fig. 6. 3D image of the optical chamber covered by reflective foil. The complex shape allows the light to be redirected towards the PMT active areas.

The optical chamber is made as a single piece, possible only with 3D printing. White PLA is used in this case, although this results in a surface that is not very reflective. Ideally, PC-PTFE, which has a good reflective index, could have been used, but tests showed that it was not possible to make an optical chamber with the mechanical and dimensional constraints necessary for its use (i.e. to be able to place the liquid scintillation vial properly inside the chamber). As a result, white PLA was used and improvements to the surface reflectivity were made using additional surface treatment, such as painting or aluminium or reflective foil coating. The chamber was first designed with the

assumption that the use of reflected light is never total, so it is better to rely solely on direct light. As it can be seen in Figs. 6 and 7, the distance between the PMT window and the vial is therefore as small as possible.

To ensure that the vial is always positioned in the same manner, a small cylindrical cut-out has been made on the bottom of the optical chamber. The radius of the cut-out is only slightly larger than the size of a standard vial, thus minimizing the possible movement of the vial inside the chamber. A drawback is that part of the bottom of the vial is not directly visible to the PMTs and some small light losses are possible. We then decided to optimise the shape of the optical chamber by treating its surface as a perfect mirror. While the upper and lower ends were modified to form a surface inclined at 45°, various geometries were tried between the PMTs. Triangular, cylindrical and flat areas between PMTs were less efficient than two concave areas to focus the photons on the PMT windows. Accordingly, in the 3D design software used here [15], we used the sketch function to trace the path of a photon using simple geometric constraints on the sketch line as shown in Fig. 7. Gross optimisation was performed assuming that the surface was a reflecting concave mirror and the changes in index between materials were neglected.

With this design, the chamber can easily be changed, which is convenient for modification and testing of new shapes and especially for testing different surface treatments to improve light reflection. We decided to use a highly reflective foil, enhanced specular reflector (ESR) [16], in order to improve the detection efficiency as will be shown in Section 3.2. This foil is commonly used for Liquid-crystal display (LCD) applications and provides a reflectivity higher than 98% for all the visible spectrum.

#### 2.5. Neutral density filters concept

There are three types of efficiency modification methods commonly used in TDCR measurements: chemical quenching, PMT defocusing, and neutral density filters [17]. However, these methods differ in the way the scintillation light is reduced.

- Efficiency variation by chemical quenching, e.g. with nitro-methane: This requires preparing a series of scintillating sources with different amounts of quenching agent. The quenching agent may act differently on the fast and the delayed fluorescence, which is not optimal. This effect was noticed with the mini-TDCR and  $^3\text{H}$  sample with different liquid scintillators in a comparison of efficiency variation by chemical quenching and neutral density filters [18].
- Changing the focusing voltage of the PMTs: This requires a fairly simple setup on the voltage divider of the PMTs but necessitates access to a focusing electrode. Moreover, this change of voltage on the PMTs directly influences their operation, which can change the active area of the photocathodes and induce an asymmetry in the detector [19].

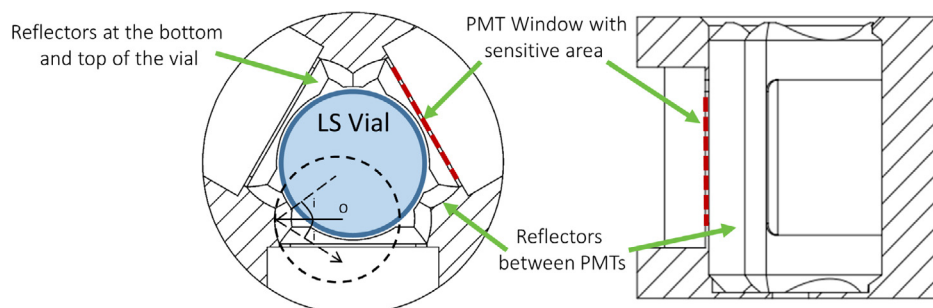


Fig. 7. Cross-section of the optical chamber, with the reflective surface treated as perfect concave mirror to optimize the shape by simple ray tracing in Solidworks [15].



- Use of neutral density filters: These filters can be inserted between the vial and the PMTs in order to reduce the number of photons reaching the PMTs, thus reducing the detection efficiency. However, they can be quite thick, which would adversely affect our optimization of the measurement system (PMTs very close to the vial). However, unlike the other two methods for varying the detection efficiency, this one does not require any modification of the photon source or the detectors.

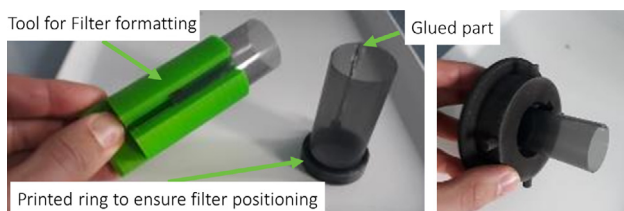


Fig. 8. On the left: picture of the filter tool, in the middle: mounted filter, and filter mounted in the cap on the right.

We have therefore designed filters with different neutral density adapted to the devices. These filters consist of a plastic film on which different levels of grey are printed by a standard laser printer. The grey areas simply correspond to a level of transparency generated by any image processing software. The sheet is then printed and cut to the desired size. The 3D printed assembly tool shown in Fig. 8 provides a cylindrical filter with a diameter suitable for the measuring device and the 20 mL liquid scintillation vial. The limitation of this assembly is the glue joint of the plastic film, as shown in Fig. 8 with a poorly glued example. In order to overcome this problem, a retaining ring with a coding device that fits into the cap of the measuring device to position this non-uniform glue joint exactly between two PMTs was designed. In this way the number of photons reaching the three PMTs is reduced to the same degree with one single sample. These tools are identical for the mini-TDCR and micro-TDCR, as they both use the same optical chamber and cap.

It is also possible to completely absorb the light coming from the sample by using an opaque filter made with a piece of BK5 tissue with  $120 \mu\text{m}$  thickness [20]. We use this to check if there is any direct detection of high energy radiation by the PMTs which was the case for Sr/Y-90 sample.

These neutral density filters have also been modified to act only on one PMT, as shown in Fig. 9. Such an option was used to increase the asymmetry of the PMTs and see if the correction algorithm was working for pure beta and pure electron capture radionuclides. The results are



Fig. 9. Filters with different neutral density. The filters shown here were designed to cover only one PMT.

described in another paper [21] where we have demonstrated that the asymmetry correction works as expected, so that non-identical PMTs can be used for the TDCR method.

## 2.6. Complete device and electronics

The complete micro-TDCR device is shown in Fig. 10. The power supplies for each device are locally-made, providing +900 V for the mini-TDCR and +1000 V for the micro-TDCR with a current of 1 mA for both. The three PMTs are powered by the same power supplies, and a voltage divider placed inside the TDCR device is used to deliver the same voltage to each PMT. For both systems, the PMTs are not selected, thus their efficiencies are not identical, but it was decided to supply them with the same voltage and to apply an asymmetry correction during the measurement analysis.

The electronics for signal processing is a nanoTDCR module [22]. This module was developed in parallel for the portable devices and was tested with the mini-TDCR. The nanoTDCR has many advantages over the reference MAC3 unit that has been implemented in many NMIs [8], which with new developments have been made, such as the ability to run four acquisitions in parallel — with two different user-selectable coincidence windows (CW) and two different user-selectable base dead-time (DT) durations. A single measurement with this device, therefore provides four results at the same time (2 CW and 2 DT). This module was used for all the results presented previously, as the nanoTDCR has been validated and compared with the MAC3 unit in studies with various radionuclides and detector systems (RCTD1 and mini-TDCR) [9,23]. The nanoTDCR thresholds were set in the valley before the single electron peak and after the thermal noise, in order to allow the detection of single photons. The settings were made using irradiated glass tubes produced in a gamma ray irradiator. The glass of the irradiated tubes has defects which turns the glass into brown colour (Fig. 11). These defect produces single photons in large quantities, up to  $4000 \text{ s}^{-1}$  with the one irradiated with the highest doses we have. These irradiated glasses allow easy adjustment of the threshold of the photomultipliers, using the nanoTDCR device.

## 2.7. Monte-Carlo Model

To meet all the needs of the measurement method (corrective factors or efficiency calculation), geometrical models for Monte Carlo simulations corresponding to both devices were created using PENELOPE 2018 code [24]. PENELOPE is known to have an accurate model for low energy electrons, positrons and photons transport [25], which allows simulation of the energy absorbed by the scintillator to perform the proper TDCR calculations. Fig. 12 shows the model with two cross-sections.

This model corresponds to a 3D representation of the mini-TDCR or micro-TDCR device. It includes all the material of the vial, cap, liquid scintillator, PMTs and optical chamber. It is important to model all the interactions between the ionizing radiation and the detector, especially to take into account scattering of high-energy gamma photons. This Monte-Carlo model calculates the energy spectrum absorbed in the scintillator for discrete energy emissions, or from a spectrum input (probability density as a function of energy), or for the full decay scheme of a given radionuclide using the PenNuc function of PENELOPE 2018. The latter uses data from the Decay Data Evaluation Project (DDEP) [26]. As an example, Fig. 13 shows the simulated absorption spectrum of  $^{18}\text{F}$  in an Ultima Gold liquid scintillator.

This simulation allows evaluation of the components of each emission produced by the decay of the radionuclide. The energy deposition in the scintillator is calculated from:

- The beta particles with a spectrum identical to  $^{18}\text{F}$  (green in Fig. 13); as expected, these electrons produce a large energy deposition. The PENELOPE input spectrum data were obtained with BetaShape 2.0 code [27];



Fig. 10. The whole set of components, including locally-made high voltage supply, can be easily handled and connected to a portable computer.



Fig. 11. Picture of the irradiated glass; the brown colour is due to a defect of the glass after exposure to Co-60 gamma rays.

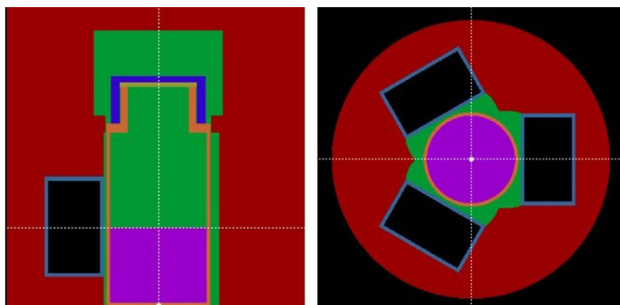


Fig. 12. Picture of the 3D model from Penelope 2018; on the left: vertical section of the system with colours corresponding to the different materials; on the right: horizontal section with the three PMTs.

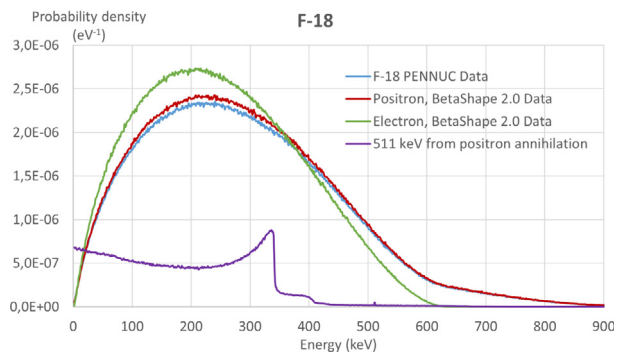


Fig. 13. Results of the PENELOPE 2018 simulation of the energy spectrum deposited in the UG scintillator by  $^{18}\text{F}$  for the micro-TDCR measurement system. The simulations were performed with different input data using PENELOPE (PenNuc or BetaShape 2.0 spectra).

- The positron annihilation (purple in Fig. 13); the Compton scattering of the 511 keV photons produces a lower energy deposition than the electrons;
- The positron particle of  $^{18}\text{F}$  (red in Fig. 13); the spectrum is broader than the one from  $\beta^-$  particles due to the stacking of the scattered photons and the positron emission spectrum. The PENELOPE input spectrum data were also obtained with BetaShape 2.0 code [27];
- $^{18}\text{F}$  (blue in Fig. 13); it has a shape almost identical to the red spectrum but this time the simulation takes into account the decay path of the radionuclide, i.e. the emission probabilities from possible electron captures (always present for  $\beta^+$  decays). The PENELOPE input data were obtained with the PenNuc module.

The first three spectra help to understand phenomena taking place in the scintillator. They give the contributions of the different types of radiation in the scintillator and help to refine the calculations for the TDCR method. The last spectrum results from the absorption of energy in the scintillator following the  $^{18}\text{F}$  decay (all emissions combined, taking into account the emission intensities). Nevertheless, this is not the spectrum to use for a TDCR measurement, as the coincident energy depositions cannot be simply added, due to the scintillator non-linearity.

Such models must be detailed in order to have the complex path of high energy electrons escaping from the vial, which may interact outside on the wall of the optical chamber and deposit only a fraction of the energy in the scintillator.

### 3. Results

#### 3.1. Neutral density filter characterisation

These filters, produced using the previously described technique, were tested in the micro-TDCR device with a  $^3\text{H}$  source in 10 mL of Ultima Gold scintillating liquid. The reduction of the  $T/D$  ratio was measured as a function of the transparency level. The results, shown in Fig. 14, prove that the filter is reducing the efficiency properly. In this test the filter level was limited to 68% transparency, as the  $T/D$  ratio becomes too small for measurements below this level.

Therefore, it is easy to produce any efficiency variation with various levels of neutral density filters. In case we need higher efficiency reduction, we can decrease the transparency of the filter quite easily.

These different levels of neutral density filters were then used to perform the efficiency variation and activity calculation on the  $^3\text{H}$  sample in order to derive the proper  $kB$  value (ionisation quenching parameter from Birks model [28]) as shown in Fig. 15.

**Table 1**

Comparison of efficiency between the RCTD1 from LNE-LNHB and the new portable devices. TiO<sub>2</sub> is for the optical chamber with titanium oxide paint on its surface, DPMTs is for diffusive PMTs, ESR is for the optical chamber with highly reflective foil on its surface.

Nuclide	TDCR values						
	RCTD1 TiO <sub>2</sub> DPMTs	mini-TDCR TiO <sub>2</sub>	mini-TDCR TiO <sub>2</sub> DPMTs	mini-TDCR ESR DPMTs	micro-TDCR TiO <sub>2</sub> DPMTs	micro-TDCR ESR DPMTs	$\Delta$ micro-TDCR vs RCTD1
<sup>14</sup> C	0.948	0.932	0.934	0.970	0.956	0.979	3%
<sup>63</sup> Ni	0.567	0.444	0.462	0.538	0.562	0.648	14%
<sup>3</sup> H	0.598	0.551	0.577	0.673	0.670	0.766	28%
<sup>55</sup> Fe*	0.325	0.289	0.317	0.361	0.428	0.455	40%
D counting rate (s <sup>-1</sup> ) of corresponding blank							
Tol PPO	7.0 (1)	11.0 (1)	10.6 (2)	8.9 (2)	10.2 (2)	9.6 (1)	36%
UG	6.0 (2)	11.6 (1)	11.0 (2)	9.2 (2)	10.2 (1)	11.4 (1)	90%
UGAB	6.0 (2)	11.6 (1)	11.4 (1)	9.5 (5)	11.1 (3)	10.3 (2)	72%

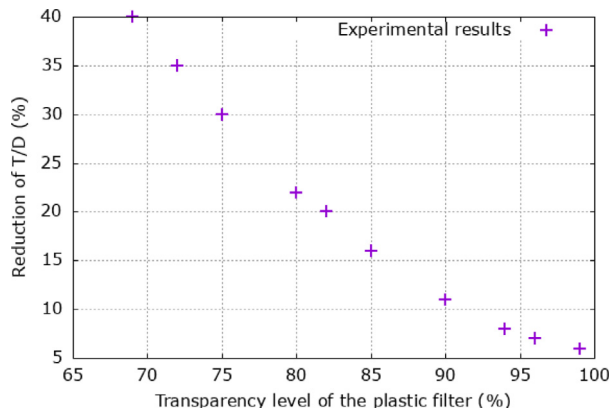


Fig. 14. Results of  $T/D$  reduction depending on the neutral density filter transparency for a <sup>3</sup>H sample in Ultima Gold and PE-PTFE vial.

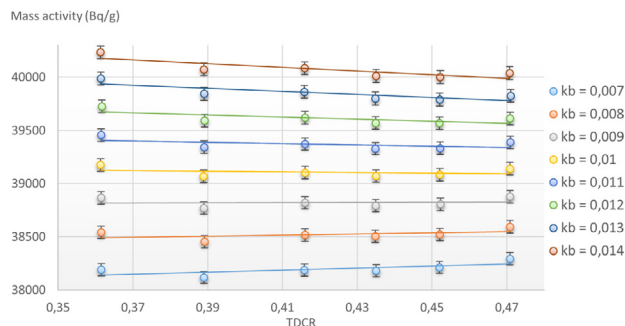


Fig. 15. Evaluation of  $kB$  for a <sup>3</sup>H sample in 10 mL of Ultima Gold liquid scintillator.

The  $kB$  value was here evaluated with a coincidence window of 40 ns and a dead time of 50  $\mu$ s. The activity was calculated with an updated version of the TDCR07c code [29] (TDCR18), yielding the results  $T/AB$ ,  $T/BC$ ,  $T/AC$  to take into account the asymmetry of the PMTs. The optimal  $kB$  value found with both the mini-TDCR and micro-TDCRs is 0.01 cm MeV<sup>-1</sup>, which is the same as the value obtained with the RCTD1 counter.

### 3.2. Response of the TDCR devices and efficiency

Table 1 shows the different TDCR values obtained for the same batch of samples during the development of the devices. The <sup>3</sup>H and <sup>14</sup>C sources were in a toluene PPO scintillator and a glass vial, the <sup>63</sup>Ni source was in UG and a glass vial, and the <sup>55</sup>Fe source was in UGAB and a PE-PTFE vial. The results were compared between RCTD1 from LNE-LNHB and the newly developed mini-TDCR and micro-TDCR with different surface reflectivity of the optical chamber. The RCTD1 is here

considered as the reference device of LNE-LNHB, it uses old Burle PMTs while today some Hamamatsu PMTs are better.

From these results we can note that the mini-TDCR has a lower efficiency than RCTD1. Even if the window of the PMTs is made diffusive in order to increase the efficiency, it still remains lower. However, this is not the case with the micro-TDCR, which has the same optical chamber as the mini-TDCR, but different PMTs. The efficiency with this device is actually higher, which shows a real improvement in the results. The reflective foil used here [16] has more than 98% reflectivity for visible light and is the best reflector found so far. We can clearly see a great improvement in the detection efficiency depending on the energy emission. While there is a little improvement at high energy, we can see that detection efficiency becomes very close to 1 for <sup>14</sup>C.

There is, however, a trade-off with these new compact devices: as shown in Table 1 they have a higher blank counting rate than the RCTD1 device. This difference is due to two phenomena: their higher efficiency and their inherent shielding. The RCTD1 device consists of an aluminium optical chamber a few centimetres thick, while the portable devices are made only of plastic with lower external radiation shielding capacity. This is nevertheless not a hindrance to the method, as standard practice is to perform a blank measurement before each sample measurement, also if necessary these portable instruments can be placed in a shielded cell, unlike other bulky instruments.

In Table 2 we present the efficiency results of both portable devices obtained for various samples measured with the devices. Here we show the  $T/D$  corresponding to each sample and the calculated activity with both devices.  $T/D$  is used as one of the indicators for the ESIR system [5] for pure beta emitters. In these results the <sup>241</sup>Pu sample contains 2.7% of <sup>241</sup>Am and the <sup>32</sup>P sample contains 1.3% of <sup>33</sup>P, and the calculated activities are corrected for these impurities. The other samples do not have any detected impurities.

All these results are presented for the mini-TDCR and micro-TDCR systems, both with reflective foil on the optical chamber surface. From these results we can clearly see the performance of the systems as well as the differences between both.

### 3.3. Comparison and validation of the systems

Samples of <sup>3</sup>H and <sup>14</sup>C in toluene PPO scintillator were measured in a glass vial using all three devices: RCTD1, mini-TDCR and micro-TDCR. The measurements were performed at LNE-LNHB. These radionuclides, commonly measured with the TDCR method, were chosen because they are low energy emitters, so their measurement is very sensitive to the detection efficiency. For each of these measurements, the activity was calculated with the TDCR18 [31] code with the measured  $T/AB$ ,  $T/BC$  and  $T/AC$  ratio measurements in order to correct for any asymmetry. For each measurement, the value  $kB = 0.010$  (1) cm MeV<sup>-1</sup> was used. The results calculated with 10 consecutive measurements are presented in Table 3.



**Table 2**

Summary of TDCR values for various radionuclides measured using both devices mini-TDCR and micro-TDCR. The activity is calculated with the same code, the nuclear data for EC radionuclides and beta spectra are calculated with BetaShape 2.0 [27,30]. The difference  $\Delta$  between the mini-TDCR and micro-TDCR is calculated as (micro-TDCR - mini-TDCR)/mini-TDCR. The vial type P stands for PTFE coated PE, G stands for glass vial, and  $G_f$  stands for frosted glass vial.

Nuclide	Cocktail	Vial	T/D values			Calculated activity (Bq)		
			mini-TDCR	micro-TDCR	$\Delta$	mini-TDCR	micro-TDCR	$\Delta$
$^{55}\text{Fe}$	UG	P	0.2992 (11)	0.4378 (12)	46.3%	3661 (20)	3678 (18)	0.46%
$^{59}\text{Ni}$	UG	P	0.31641 (44)	0.5415 (8)	71.1%	533.1 (39)	539.5 (26)	1.2%
$^{241}\text{Pu}$	UG	P	0.4925 (3)	0.5961 (8)	21.0%	770 (8)	770 (8)	0.02%
$^3\text{H}$	UG AB	P	0.40387 (8)	0.5543 (11)	37.2%	3714 (15)	3707 (9)	-0.19%
$^3\text{H}$	TOL PPO	G	0.6731 (14)	0.7675 (11)	14.0%	408.2 (16)	408.7 (16)	0.12%
$^{125}\text{I}$	UG	P	0.7146 (7)	0.7955 (11)	11.3%	639 (6) (5)	639 (6)	-0.09%
$^{63}\text{Ni}$	UG AB	G	0.77657 (47)	0.85620 (41)	10.3%	3591 (7)	3596.9 (49)	0.16%
$^{35}\text{S}$	UG	G	0.93130 (12)	0.95282 (38)	2.3%	8496 (7)	8494 (7)	-0.02%
$^{60}\text{Co}$	UG	G	0.96368 (42)	0.97827 (14)	1.5%	5523 (11)	5520 (11)	0.01%
$^{14}\text{C}$	TOL PPO	G	0.96794 (44)	0.9792 (6)	1.2%	1660.5 (33)	1660.5 (17)	0.00%
$^{90}\text{Sr}/\text{Y}$	HF	G	0.98520 (19)	0.98933 (30)	0.4%	5067 (15)	5055 (15)	-0.24%
$^{32}\text{P}$	UG	G	0.99607 (36)	0.99744 (39)	0.1%	5097 (20)	5109 (20)	0.23%
$^{233}\text{U}$	UG AB	$G_f$	0.99554 (22)	0.99944 (11)	0.4%	7160 (7)	7165 (7)	0.07%
$^{238}\text{Pu}$	HF	G	1.0000 (6)	1.00003 (40)	0.03%	2515.0 (25)	2513.9 (25)	-0.07%
$^{241}\text{Am}$	HF	G	1.0003 (8)	1.00001 (34)	0.03%	1738.4 (13)	1738.6 (6)	0.01%

**Table 3**

Comparison between RCTD1, mini-TDCR and micro-TDCR for  $^3\text{H}$  and  $^{14}\text{C}$  samples. The difference  $\Delta$  is calculated as a relative difference from RCTD1.

	Activity $^{14}\text{C}$ (Bq)	$\Delta$	Activity $^3\text{H}$ (Bq)	$\Delta$	Blank D count rate ( $\text{s}^{-1}$ )	$\Delta$
Micro-RCTD	6400 (6)	0.22%	1060 (5)	0.43%	10.21 (5)	45%
Mini-RCTD	6392 (13)	0.10%	1056 (7)	0.00%	10.6 (2)	51%
RCTD1	6386 (13)	-	1056 (7)	-	7.0 (1)	-

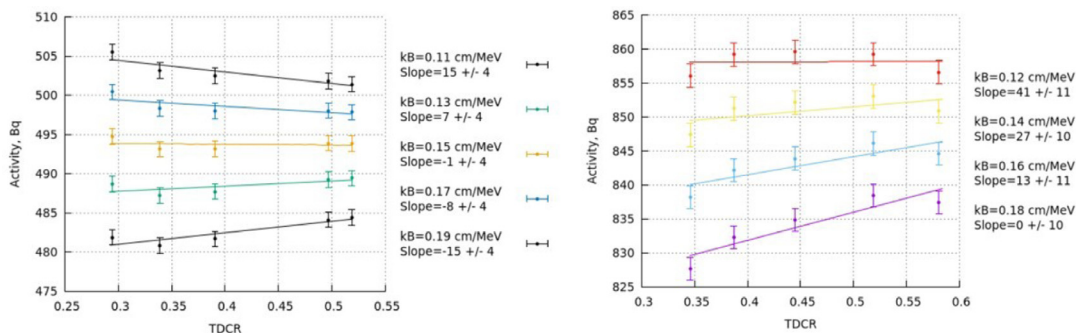


**Fig. 16.** Efficiency variation of the TDCR-SU detector with the LKB  $^3\text{H}$  N#1 source (left) and of the mini-TDCR detector with LKB  $^3\text{H}$  N#2 (right).

A slight difference can be observed in the results. It seems to be correlated to the efficiency of the devices, the higher the efficiency, the higher the activity of the final result. However, this variation is not significant in view of the measurement uncertainties, as all the results are coherent. This comparison allows us to validate the proper operation of our new devices in comparison with the RCTD1 counter.

The mini-TDCR device was then moved to Sofia University, in order to perform a comparison with the portable device, called TDCR-SU [9]. This portable TDCR uses the same PMTs as the mini-TDCR, but the optical chamber is made of PTFE and has a different shape. The main difference is that the PMTs are not placed as close to the vial as in the mini-TDCR. The sources measured in this experiment were two standard Wallac sources ( $^3\text{H}$  and  $^{14}\text{C}$ ) and two sources calibrated by LNE-LNHB and RCTD1 in 2008 (LKB  $^3\text{H}$  N#2 and Amersham  $^{14}\text{C}$ ). All sources were in a toluene based cocktail in glass vials covered by diffusive tape. One of the  $^{14}\text{C}$  sources was measured with and without diffusive tape, but the difference in the calculated activity was less than 0.08%.

The LKB  $^3\text{H}$  source N#2 was measured in the past with mesh filters on the TDCR-SU, and it was noticed that the optimal  $kB$  value was abnormally high (above 0.018 cm MeV $^{-1}$ ), indicating some problems with the sample or the measurement. In order to identify the cause of this issue, it was decided to measure this sample with various neutral

density filters in the mini-TDCR. The efficiency variation method with the same neutral density filters also was performed also on the LKB  $^3\text{H}$  source N#1 with the TDCR-SU detector in order to see if the problem came either from the TDCR-SU or from the filters. The results are presented in Fig. 16.

From this analysis we can see that the  $kB$  obtained with the LKB  $^3\text{H}$  N#1 source is 0.015 cm MeV $^{-1}$  with the TDCR-SU (similar to the value with that device system and the mesh filters). There is no problem in the  $kB$  evaluation in this case. However, we again found the same unexpectedly high value of  $kB$  for the LKB  $^3\text{H}$  N#2 source, confirming that the problem is with this sample. Table 4 summarizes the comparison between each device for the different sources.

One can see a difference in the detection efficiencies between both devices. Whilst it is less than 1% for the  $^{14}\text{C}$  samples, it increases to almost 12% for the  $^3\text{H}$  sample. This shows that the design, material and reflectivity of the chamber, have a major impact on the efficiency. It should also be noted that at the time of this comparison, the mini-TDCR chamber was painted with  $\text{TiO}_2$  paint, rather than lined with an ESR foil, as is now the case, so the detection efficiency is now higher as shown in Table 1. The Table 5 shows the  $D$  count rate of each blank sample, the LKB N#1 is the blank for LKB  $^3\text{H}$  N#1 and LKB  $^{14}\text{C}$ . We can observe an increase in the blank  $D$  count rate on the sample in the mini-TDCR compared to the TDCR-SU. This increase seems to

**Table 4**  
Comparison between the mini-TDCR and the portable TDCR-SU for  $^3\text{H}$  and  $^{14}\text{C}$  samples.

Samples	$kB$ ( $\text{cm MeV}^{-1}$ )	TDCR-SU		Mini-TDCR		Relative difference	
		Efficiency	Activity (Bq)	Efficiency	Activity (Bq)	Efficiency	Activity (Bq)
LKB, $^3\text{H}$ , №1	0.013	0.5594	489.4 (24)	0.6251	490.5 (25)	11.7%	0.23%
	0.015	0.5544	493.8 (25)	0.6201	494.5 (25)	11.9%	0.13%
LKB, $^3\text{H}$ , №2	0.013	0.5557	839 (7)	0.6182	841 (6)	11.3%	0.29%
	0.018	0.5440	857 (7)	0.6070	8576 (6)	11.6%	0.00%
LKB, $^{14}\text{C}$	0.010	0.9547	1779.4 (36)	0.9630	1780.0 (36)	0.87%	0.03%
Amersham, $^{14}\text{C}$	0.010	0.9531	544.1 (20)	0.9600	543.9 (20)	0.72%	-0.03%

**Table 5**  
D count rate for each blank sample and both TDCR devices.

Blank sample	TDCR-SU	mini-TDCR	Relative deviation
LKB №1	13.25 (6)	14.21 (6)	7.2%
LKB №2	13.13 (5)	14.10 (9)	7.4%
Amersham	17.10 (7)	19.18 (8)	12.2%

**Table 6**  
Comparison between mini-TDCR and the portable TDCR-SU for  $^3\text{H}$  and  $^{14}\text{C}$  samples.

Samples	Device	Activity (Bq)		Relative deviation
		Measurement	Certificate	
LKB, $^3\text{H}$ , №2	TDCR-SU	839 (7)	835 (8)	0.40%
	Mini-TDCR	841 (6)		0.69%
Amersham, $^{14}\text{C}$	TDCR-SU	544.1 (20)	543.9 (11)	0.03%
	Mini-TDCR	543.9 (20)		0.00%

be due to the difference in detection efficiency as both devices are unshielded and both are made of some centimetres of plastic only. The difference of the background compared to the results obtained in the LNE-LNHB laboratory can be explained by the verified higher indoor radon concentration in Sofia University compared to that in LNE-LNHB, which is due to the soil composition.

The activities obtained in this experiment were compared with the certified activity and the results are presented in Table 6. Good agreement can be seen between the current measurements and the source certificates.

We must note that, as confirmed by the filter measurements, the LKB  $^3\text{H}$  №2 sample shows a high  $kB$  and may be compromised.

### 3.4. On-site test for high activity and half-life measurement

Measurements were performed in the Orsay Hospital in CEA/SHFJ (Service Hospitalier Frédéric Joliot), where  $^{11}\text{C}$  and  $^{18}\text{F}$  are produced for PET imaging. The aim was both to check the linearity of our device during the measurements and to show that it is possible to use the device to measure the presence or absence of impurities in the solution. These measurements were carried out on samples of  $^{11}\text{C}$  and  $^{18}\text{F}$  prepared from spare ready to inject solutions mixed with Ultima Gold scintillating cocktail. Thanks to the quality control performed by SHFJ, we knew that these colloidal solutions were free from impurities. Successive series of measurements were carried out on these two samples. Follow-up counting rates of the logical sum of double coincidences are presented in Fig. 17. These results were obtained with a coincidence window of 40 ns and a dead-time of 50  $\mu\text{s}$ .

All counting rates are corrected for accidental coincidences according to the methodology proposed in [32], which represents a correction of the order of 0.03% to 0.04% for  $^{11}\text{C}$  and 0.03% to 0.15% for  $^{18}\text{F}$ . For these radionuclides, the detection efficiency is high, leading to a low proportion of accidental coincidences despite the high count rate. The highest accidental coincidence corrections occur when the counting rate is the highest and again when the counting rate is close to the background counting rate. The smallest corrections are obtained for activity between 10 kBq and 20 kBq, which could be regarded

as the optimum activity value in order to minimize the accidental coincidence correction for an activity measurement with this device and these two radionuclides. The series of measurements performed for both radionuclides were fitted with Eq. (1):

$$f(x) = D_0 e^{\left(\frac{-\ln(2)t}{T_{1/2}}\right)} + D_{Blk} \quad (1)$$

Where,  $D_{Blk}$  is the background counting rate,  $D_0$  is the counting rate at the beginning of the experiment,  $t$  is the time and  $T_{1/2}$  is the measured half-life. The fitting is performed with  $\chi^2$  minimization using the non-linear least squares Levenberg–Marquardt algorithm implemented in Gnuplot [33].

The result obtained for  $^{11}\text{C}$ , 20.333 (7) min, is consistent with the DDEP value of 20.361 (23) min [34]. In a similar way, the counting analysis was carried out for the  $^{18}\text{F}$  sample; the half-life thus measured was 1.82870 (20) h, in excellent agreement with the DDEP value 1.827890 (23) h [35]. The uncertainty presented here correspond only to the fit uncertainty, a complete study of the half-life measurements and corresponding uncertainty budgets will be presented in another publication.

It is especially important to note that the first measurements were carried out with an extremely high count rate of 430 000  $\text{s}^{-1}$ . These measurements were performed down to 160  $\text{s}^{-1}$ , thereby demonstrating that the micro-TDCR combined with nanoTDCR device can operate over a very wide range of counting rates with very good linearity of the detection device. An impurity measurement was also performed after the total decay of the  $^{11}\text{C}$  (24 h) and  $^{18}\text{F}$  (7 days) respectively with liquid scintillation. The counting rate obtained  $D = 4.85$  (8)  $\text{s}^{-1}$  corresponds to the rate from the blank vial,  $D = 4.87$  (8)  $\text{s}^{-1}$ , so no long-lived radionuclides were present in the samples, as we could suspect the presence of  $^3\text{H}$ . From these results, we deduced that the solution is free of impurities, the Table 7 presents the activity and activity concentration measurement results. The uncertainty of the measured volume is quite large compared to typical high precision mass measurements such as performed in the metrology laboratory, which are not feasible in the hospital. This explains the higher-than-normal uncertainty of the activity concentration.

The uncertainty budget also shows the importance of the exact measurement time, which is critical for the measurement of  $^{11}\text{C}$ . Its short half-life has a huge impact on the results considering the chosen reference time. It should be noted that no access to an internet time server was possible during this measurement, and the corresponding uncertainty component could be eliminated if a time server were available. On the other hand, while  $^{18}\text{F}$  has a longer half-life, there are some non-negligible electron capture decays that increase the uncertainty arising from the decay data. For activity calculation with the TDCR model, we used the results of PENELOPE 2018 simulations in order to get the interaction probability of 511 keV (Fig. 13). The calculated detection efficiency with the fully detailed model was 0.07% lower compared to a simple vial model.

### 3.5. On-site test for low activity and radon calibration

A first test, dedicated to in-situ measurement of radon in water, was performed at the Institut de Radioprotection et Sureté Nucléaire (IRSN)

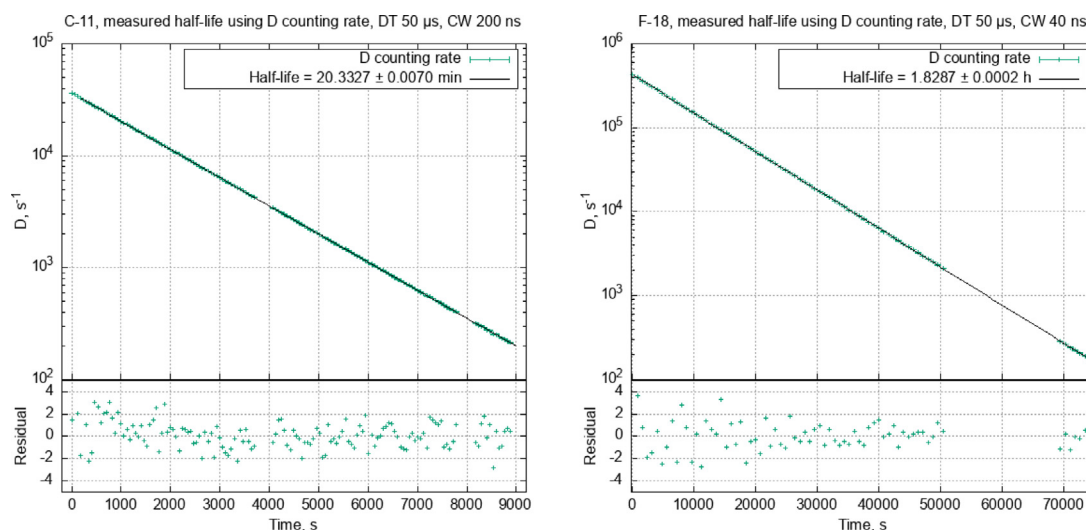


Fig. 17. Measurement of  $^{18}\text{F}$  and  $^{11}\text{C}$  half life on-site, the uncertainties correspond only to fitting adjustment and boundaries. The residuals are defined as the difference between experimental double counting rate and the fit function that was then divided by the standard deviation.

Table 7

Results of activity concentration measurements for  $^{18}\text{F}$  and  $^{11}\text{C}$  with their corresponding uncertainty budget.

	Relative standard uncertainty $^{18}\text{F}$	Relative standard uncertainty $^{11}\text{C}$
Coincidence window	0.01%	0.02%
Dead time	0.01%	0.01%
Counting statistics	0.03%	0.05%
Blank	0.01%	0.04%
Time	0.33%	0.17%
Beta spectra	0.11%	0.01%
Decay data other than Beta spectra	0.20%	0.01%
Efficiency calculation (including $kB$ )	0.10%	0.10%
Accidental coincidences	0.02%	0.02%
Decay during measurement	0.004%	0.002%
Decay correction to a reference time	0.02%	0.32%
<b>Combined uncertainty of activity</b>	<b>0.41%</b>	<b>0.38%</b>
Volume	1.10%	0.90%
<b>Combined uncertainty of volumic activity</b>	<b>1.2%</b>	<b>1.0%</b>
<b>RESULT, activity concentration (MBq ml<math>^{-1}</math>)</b>	<b>82.3 (10)</b>	<b>9.47 (9)</b>



Fig. 18. Picture of the micro-TDCR device inside the shielding from an HPGe detector.

in the framework of their proficiency test preparation [36]. The final goal was to calibrate their commercial scintillation detectors.

The problem of  $^{222}\text{Rn}$  in water is mainly related, apart from the measurement itself, to the preparation, transport and storage of liquid scintillation samples. The gas has its own behaviour in the water/scintillator mixture and can escape from the sample. By performing primary measurements in-situ on samples prepared directly within the laboratory, we eliminated all these problems and were able to directly calibrate the secondary scintillation devices. To do this, the micro-TDCR device was transported to the Environmental Analysis and

Metrology Service of the IRSN/Vésinet and set up inside a shield as show in Fig. 18. This shielding was developed for an HPGe detector, but the small size of the micro-TDCR device, allows it to be placed inside the shielding in order to reduce the background. The shielding was composed of 10 cm of low-level lead and 2 mm of copper. This type of shielding is widely used for the measurement of environmental samples in gamma-ray spectrometry and allowed us to reduce the  $D$ -count rate for the samples from 23.8 (1)  $\text{s}^{-1}$  to 2.1 (1)  $\text{s}^{-1}$ . The samples were prepared in a 20 mL PE-PTFE coated liquid scintillation vials with 10 mL of radon-loaded water (deionized water for the blank) and the rest of the volume filled with UG LLT scintillator.

The measurements were performed the day after the preparation of the samples and radon spiking, so equilibrium was reached between radon and decay products. Due to the long half-life of  $^{210}\text{Pb}$  (22.23 (12) years), the decay scheme process is considered to be stopped at this radionuclide; in the present case it represents only 0.008% of the radon activity. Using the decay data, we can calculate the equilibrium ratio between  $^{222}\text{Rn}$  and its progenies up to  $^{210}\text{Pb}$  (considered stable in our case). This ratio is 5.025, i.e. for one radon decay there are 5.025 detectable events in liquid scintillation with an almost unitary detection efficiency as they are high energy alpha or beta particles.

However, one of the decay product of radon has a short half-life ( $T_{1/2}(^{214}\text{Po}) = 162.3 \mu\text{s}$ ), comparable to the dead time of the electronics. As demonstrated in [37], several measurements with different

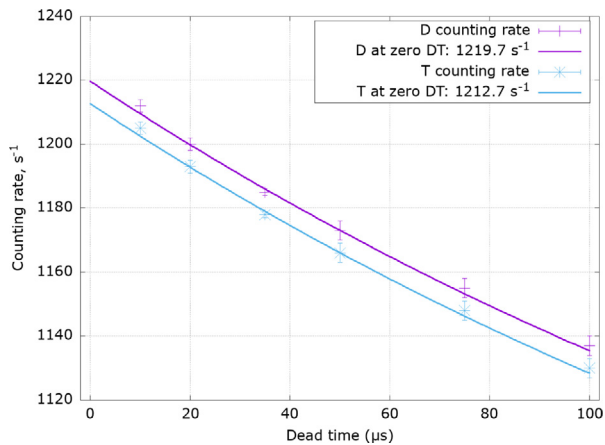


Fig. 19. Analysis of the results obtained with different dead time and extrapolation.

dead-times must be performed in order to extrapolate the counting results to zero dead-time with Eq. (2).

$$f(x) = a + be^{\left(\frac{-\ln(2)x}{T_{1/2}(P_{\alpha}-214)}\right)} \quad (2)$$

The results with different dead times are presented in Fig. 19. The  $D$  and  $T$  counting rates were calculated for a dead time equal to zero using the values obtained from the fit with Eq. (2).

These measurements allowed us to calculate the activity of the samples prepared by the IRSN with the method from [37]. The detection efficiency was determined with the  $T/D$  value obtained at zero dead time with Betashape 2.0 [27] spectra and considering the detection efficiency for alpha equal to 1. The calculation took into account the relative quantum efficiencies of the PMTs. The detection efficiency obtained for  $D$  is 5.0108 for radon at equilibrium with its daughter and with  $kB = 0.01 \text{ cm MeV}^{-1}$ . The main compound of the uncertainty budget arises from the fitting results of the zero dead time extrapolation. The calculated activity of this sample is 243.4 (24) Bq of  $^{222}\text{Rn}$ , this value was used by IRSN to calibrate their Tricarb LS counter.

#### 4. Conclusions

The two devices developed and manufactured at LNE-LNHB are now operational and have been validated by various comparisons and in-situ measurement tests. These devices are not only portable, but also more efficient than the historical device (RCTD1) of LNE-LNHB, especially in the case of the micro-TDCR which is the smallest of the devices. The optimization of the chamber's shape was done with our only available tool at the beginning of the device development but we believe there is still potential to increase the detection efficiency when using advanced ray-tracing tools based on a comprehensive physical model. The devices provide more flexibility for testing, as we can easily 3D-print different optical chambers or specific tools. As a result, the mini-TDCR and micro-TDCR were also used in various experiments and collaborations in order to improve the TDCR method, such as the compact electronic module nanoTDCR [23,38], optimal coincidence windows [18], accidental coincidence correction [32], PMT asymmetry [21], measurement of the half-life of excited nuclear states [39] and new studies on the time domain in liquid scintillation [40]. The multiple experiments presented here have demonstrated the very good capability and detection efficiency of such complete devices, in particular with excellent linearity for counting rates from  $430\,000 \text{ s}^{-1}$  to  $160 \text{ s}^{-1}$ . We also demonstrated the significance of such portable devices, for example for the measurements in a secondary environmental laboratory, in particular for radon, which allows source preparation and/or transportation difficulties to be overcome for this radionuclide.

We believe that such devices, which are now commonly used in our laboratory for liquid scintillation measurements, are of great interest in order to perform on-site comparison measurements or for a possible future portable Extended International Reference System for pure  $\beta$ -particle emitting radionuclide (ESIR) devices. Finally, following these developments the work will now focus on two areas: firstly to develop the Compton-TDCR device, secondly to combine the portable TDCR with on-site source preparation using direct volume measurement.

#### CRedit authorship contribution statement

**Benoît Sabot:** Investigation, Methodology, Design, Monte-Carlo, Funding acquisition, Experiments, Writing – original draft. **Chavdar Dutsov:** Investigation, Software, Formal analysis, Experiments, Manuscript review. **Philippe Cassette:** Supervision, Conceptualization, Experiments, Methodology, Manuscript review. **Krasimir Mitev:** Resources, Formal analysis, Experiments, Manuscript review.

#### Declaration of competing interest

The authors declare that they have no known competing financial interests or personal relationships that could have appeared to influence the work reported in this paper.

#### Acknowledgements

This work was funded by the French national metrology institute: Laboratoire National de Métrologie et d'Essais (LNE). The authors thank them for providing all the funds which were required to build the setup and perform the various studies linked to this project. The authors thank Philippe Gervais and Anne-Laure Teppe for their assistance, for the supply of  $^{11}\text{C}$  and  $^{18}\text{F}$ , and for having allowed us to carry out these experiments at CEA/SHFJ (Orsay Hospital) under very good conditions. The authors thank Vadim Tsoupko-Sitnikov for the radon experiments at IRSN. Finally, the authors thank Margot Corbel and Sophie Morelli for some of the source preparation and Mark A. Kellett, Carole Fréchou, Christophe Dulieu and Marie-Christine Lépy for their useful comments on the document.

#### References

- [1] R. Broda, P. Cassette, K. Kossert, Radionuclide metrology using liquid scintillation counting, *Metrologia* 44 (4) (2007) S36, <http://dx.doi.org/10.1088/0026-1394/44/4/S06>.
- [2] P. Cassette, M. Capogni, L. Johansson, K. Kossert, O. Nähle, J. Sephton, P.D. Felice, Development of Portable Liquid Scintillation Counters for On-Site Primary Measurement of Radionuclides Using the Triple-to-Double Coincidence Ratio Method, *IEEE*, 2013, <http://dx.doi.org/10.1109/animma.2013.6727876>.
- [3] F. Republic, URL <https://www.legifrance.gouv.fr/jorf/id/JORFTEXT000019907487>.
- [4] F. Republic, URL <https://www.legifrance.gouv.fr/eli/arrete/2017/2/23/DEVR1635310A/JO/texte>.
- [5] R. Coulon, S. Judge, H. Liu, C. Michotte, The international reference system for pure beta-particle emitting radionuclides: An evaluation of the measurement uncertainties, *Metrologia* 58 (2) (2021) 025007, <http://dx.doi.org/10.1088/1681-7575/abe355>.
- [6] BIPM, The SIRT : A new Tool Developed at the BIPM for Comparing Activity Measurements of Short-Lived Radionuclides World-Wide, (Rapport BIPM-2013/02) Bureau International des Poids et Mesures, 2013, Accessed on 11.25.2021, URL <https://www.bipm.org/documents/>.
- [7] P. Cassette, R. Vatin, Experimental evaluation of TDCR models for the 3 PM liquid scintillation counter, *Nucl. Instrum. Methods Phys. Res. A* 312 (1–2) (1992) 95–99, [http://dx.doi.org/10.1016/0168-9002\(92\)90135-q](http://dx.doi.org/10.1016/0168-9002(92)90135-q).
- [8] J. Bouchard, P. Cassette, MAC3: an electronic module for the processing of pulses delivered by a three photomultiplier liquid scintillation counting system, *Appl. Radiat. Isot.* 52 (3) (2000) 669–672, [http://dx.doi.org/10.1016/S0969-8043\(99\)00228-6](http://dx.doi.org/10.1016/S0969-8043(99)00228-6).
- [9] K. Mitev, P. Cassette, V. Jordanov, H.R. Liu, C. Dutsov, Design and performance of a miniature TDCR counting system, *J. Radioanal. Nucl. Chem.* 314 (2) (2017) 583–589, <http://dx.doi.org/10.1007/s10967-017-5451-3>.



- [10] P. Cassette, P. Do, The Compton source efficiency tracing method in liquid scintillation counting: A new standardization method using a TDCR counter with a Compton spectrometer, *Appl. Radiation Isot.* 66 (6–7) (2008) 1026–1032, <http://dx.doi.org/10.1016/j.apradiso.2008.02.062>.
- [11] Volumic3D, Volumic3D FDM Printer, Volumic & GEMEA, 2016, Accessed on 11.04.2021, URL <https://imprimante-3d-volumic.com/>.
- [12] Hamamatsu, Photomultiplier Tubes R7600U Series, Hamamatsu photonics, 2016, Accessed on 03.02.2022, URL <https://www.hamamatsu.com/eu/en/product/type/R7600U-20/index.html>.
- [13] Hamamatsu, Photomultiplier Tubes - Basics and Application, Hamamatsu photonics, 2007, Accessed on 03.02.2022, URL [https://www.hamamatsu.com/content/dam/hamamatsu-photonics/sites/documents/99\\_SALES\\_LIBRARY/etd/PMT\\_handbook\\_v3aE.pdf](https://www.hamamatsu.com/content/dam/hamamatsu-photonics/sites/documents/99_SALES_LIBRARY/etd/PMT_handbook_v3aE.pdf).
- [14] Hamamatsu, Photomultiplier Tubes R11265U and H11934 Series, Hamamatsu photonics, 2019, Accessed on 11.04.2021, URL [https://www.hamamatsu.com/resources/pdf/etd/R11265U\\_H11934\\_TPMH1336E.pdf](https://www.hamamatsu.com/resources/pdf/etd/R11265U_H11934_TPMH1336E.pdf).
- [15] D. Systèmes, Solidworks User Manuel, Dassault Systèmes, 2020, Accessed on 11.04.2021, URL <https://help.solidworks.com/>.
- [16] 3M, 3M Enhanced Specular Reflector (3M ESR), 3M, 2021, Accessed on 16.05.2021, URL [https://www.3m.com/3M/en\\_US/p/d/eebgdar000006/](https://www.3m.com/3M/en_US/p/d/eebgdar000006/).
- [17] P. Cassette, R. Broda, D. Hainos, T. Terlikowska, Analysis of detection efficiency variation techniques for the implementation of the TDCR method in liquid scintillation counting, *Appl. Radiat. Isot.* 52 (3) (2000) 643–648, [http://dx.doi.org/10.1016/S0969-8043\(99\)00224-9](http://dx.doi.org/10.1016/S0969-8043(99)00224-9).
- [18] C. Dutsov, P. Cassette, K. Mitev, B. Sabot, In quest of the optimal coincidence resolving time in TDCR LSC, *Nucl. Instrum. Methods Phys. Res. A* (2020) 164846, <http://dx.doi.org/10.1016/j.nima.2020.164846>.
- [19] P. Arenillas, P. Cassette, Implementation of the TDCR liquid scintillation method at CNEA-LMR, Argentina, *Appl. Radiat. Isot.* 64 (10–11) (2006) 1500–1504, <http://dx.doi.org/10.1016/j.apradiso.2006.02.091>.
- [20] Blackout and Laser Safety Materials, Thorlabs, 2018, Accessed on 11.04.2021, URL [https://www.thorlabs.com/newgrouppage9.cfm?objectgroup\\_id=190&pn=BK5](https://www.thorlabs.com/newgrouppage9.cfm?objectgroup_id=190&pn=BK5).
- [21] K. Kossert, B. Sabot, P. Cassette, R. Coulon, H. Liu, On the photomultiplier-tube asymmetry in TDCR systems, *Appl. Radiat. Isot.* 163 (2020) 109223, <http://dx.doi.org/10.1016/j.apradiso.2020.109223>.
- [22] nanoTDCR Triple-to-Double Coincidence Ratio Liquid Scintillation Counting System (TDCR) and MCA Manual, Yantel, 2019, URL [https://www.yantel.com/wp-content/uploads/nanoTDCR\\_TD9009\\_TD9010\\_Data\\_Sheet\\_Rev\\_01Cs.pdf](https://www.yantel.com/wp-content/uploads/nanoTDCR_TD9009_TD9010_Data_Sheet_Rev_01Cs.pdf).
- [23] V. Jordanov, P. Cassette, C. Dutsov, K. Mitev, Development and applications of a miniature TDCR acquisition system for in-situ radionuclide metrology, *Nucl. Instrum. Methods Phys. Res. A* 954 (2020) 161202, <http://dx.doi.org/10.1016/j.nima.2018.09.037>.
- [24] F. Salvat, J.M. Fernández-Varea, J. Sempau, PENELOPE-2018: A code system for Monte Carlo simulation of electron and photon transport, *NEA/MBDAV/R(2019)1* (2019) <http://dx.doi.org/10.1787/32da5043-en>, OCDE, NEA Data Bank.
- [25] M. Asai, M.A. Cortés-Giraldo, V. Giménez-Alventosa, V.G. Gómez, F. Salvat, The PENELOPE physics models and transport mechanics. Implementation into Geant4, *Front. Phys.* 9 (2021) <http://dx.doi.org/10.3389/fphy.2021.738735>.
- [26] M.A. Kellett, O. Bersillon, The decay data evaluation project (DDEP) and the JEFF-3.3 radioactive decay data library: Combining international collaborative efforts on evaluated decay data, in: A. Plompen, F.-J. Hamsch, P. Schillebeeckx, W. Mondelaers, J. Heyse, S. Kopecky, P. Sieglar, S. Oberstedt (Eds.), *EPJ Web Conf.* 146 (2017) 02009, <http://dx.doi.org/10.1051/epjconf/201714602009>.
- [27] X. Mougeot, Betashape: A new code for improved analytical calculations of beta spectra, *EPJ Web Conf.* 146 (2015) (2017) <http://dx.doi.org/10.1051/epjconf/201714612015>.
- [28] J.B. Birks, *The Theory and Practice of Scintillation Counting*, Pergamon Press, Oxford, 1964.
- [29] P. Cassette, Detection Efficiency Calculation for Pure-Beta Radionuclides, Program with Short Tutorial, LNHB, 2022, Accessed on 03.03.2022, [http://www.lnhb.fr/icrm\\_lsc\\_software/](http://www.lnhb.fr/icrm_lsc_software/).
- [30] X. Mougeot, Towards high-precision calculation of electron capture decays, *Appl. Radiat. Isot.* 154 (2019) 108884, <http://dx.doi.org/10.1016/j.apradiso.2019.108884>.
- [31] P. Cassette, TDCR; Detection Efficiency Calculation for Pure-Beta Radionuclides, Laboratoire National Henri Becquerel, 2018, Accessed on 11.25.2021, URL [http://www.lnhb.fr/icrm\\_lsc\\_software/](http://www.lnhb.fr/icrm_lsc_software/).
- [32] C. Dutsov, P. Cassette, B. Sabot, K. Mitev, Evaluation of the accidental coincidence counting rates in TDCR counting, *Nucl. Instrum. Methods Phys. Res. A* 977 (2020) 164292, <http://dx.doi.org/10.1016/j.nima.2020.164292>.
- [33] gnuplot, Gnuplot Fitting Algorithms Manual, gnuplot, 2020, Accessed on 16.05.2021, URL [http://gnuplot.sourceforge.net/docs\\_4.2/node82.html](http://gnuplot.sourceforge.net/docs_4.2/node82.html).
- [34] V. Chisté, M.M. Bé, Table des radionucléides C-11, Table Radionucléides (2011) Accessed on 01.04.2022, [http://www.lnhb.fr/nuclides/C-11\\_tables.pdf](http://www.lnhb.fr/nuclides/C-11_tables.pdf).
- [35] V. Chisté, M.M. Bé, N. Kuzmenko, Table des radionucléides F-18, Table Radionucléides (2014) Accessed on 01.04.2022, [http://www.lnhb.fr/nuclides/F-18\\_tables.pdf](http://www.lnhb.fr/nuclides/F-18_tables.pdf).
- [36] V. Tsoumpko-Sitnikov, Results of the Proficiency Test 163 RN 300, *IRSN Report, 2020-00384, Environmental Analysis and Metrology Department, IRSN, 2020*.
- [37] P. Cassette, M. Sahagia, L. Grigorescu, M.C. Lépy, J.L. Pico, Standardization of  $^{222}\text{Rn}$  by LSC and comparison with  $\alpha$ - and  $\gamma$ -spectrometry, *Appl. Radiat. Isot.* 64 (10–11) (2006) 1465–1470, <http://dx.doi.org/10.1016/j.apradiso.2006.02.068>.
- [38] C. Dutsov, K. Mitev, P. Cassette, V. Jordanov, Study of two different coincidence counting algorithms in TDCR measurements, *Appl. Radiat. Isot.* 154 (2019) 108895, <http://dx.doi.org/10.1016/j.apradiso.2019.108895>.
- [39] C. Dutsov, B. Sabot, P. Cassette, K. Mitev, Measurement of the half-life of excited nuclear states using liquid scintillation counting, *Appl. Radiat. Isot.* 176 (2021) 109845, <http://dx.doi.org/10.1016/j.apradiso.2021.109845>.
- [40] K. Mitev, C. Dutsov, P. Cassette, B. Sabot, Time-domain based evaluation of detection efficiency in liquid scintillation counting, *Nature, Sci. Rep.* 11 (1) (2021) <http://dx.doi.org/10.1038/s41598-021-91873-1>.